

Loss of habenular *Prkar2a* reduces hedonic eating and increases exercise motivation

Edra London, ... , Chris J. McBain, Constantine A. Stratakis

JCI Insight. 2020. <https://doi.org/10.1172/jci.insight.141670>.

Research In-Press Preview Metabolism Neuroscience

The habenula (Hb) is a bilateral, evolutionarily conserved epithalamic structure connecting forebrain and midbrain structures that has gained attention for its roles in depression,(1) addiction,(2-5) rewards processing,(6) and motivation (7,8). Of its two major subdivisions, the medial (MHb) and lateral Hb (LHb), MHb circuitry and function is poorly understood relative to LHb (9). *Prkar2a* codes for cAMP-dependent protein kinase (PKA) regulatory subunit II α (RII α), a component of the PKA holoenzyme at the center of one of the major cell-signaling pathways conserved across systems and species. Type 2 regulatory subunits (RII α , RII β) determine the subcellular localization of PKA, and unlike other PKA subunits, *Prkar2a* has minimal brain expression except in the MHb (10). We previously showed that RII α knockout (RII α KO) mice resist diet-induced obesity (DIO) (11). In the present study, we report that RII α KO mice have decreased consumption of palatable, “rewarding” foods and increased motivation for voluntary exercise. *Prkar2a* deficiency led to decreased habenular PKA enzymatic activity and impaired dendritic localization of PKA catalytic subunits in MHb neurons. Re-expression of *Prkar2a* in the Hb rescued this phenotype confirming differential roles for *Prkar2a* in regulating the drives for palatable foods and voluntary exercise. Our findings show that in the MHb decreased PKA signaling and dendritic PKA activity decrease motivation for food rewards while enhancing the motivation for exercise, a desirable combination of [...]

Find the latest version:

<https://jci.me/141670/pdf>



1 **Loss of habenular *Prkar2a* reduces hedonic eating and increases exercise motivation**

2

3 Edra London¹, Jason C. Wester², Michelle Bloyd¹, Shelby Bettencourt¹, Chris J. McBain², Constantine A.
4 Stratakis¹

5

6 ¹*Section on Endocrinology and Genetics, Eunice Kennedy Shriver National Institute for Child Health and*
7 *Human Development, National Institutes of Health, Bethesda, MD 20892;* ² *Section on Cellular and*
8 *Synaptic Physiology, Eunice Kennedy Shriver National Institute for Child Health and Human Development,*
9 *National Institutes of Health, Bethesda, MD 20892*

10

11 Corresponding author: Edra London

12 10 Center Drive, Bldg 10/CRC, room #1-3216E

13 Bethesda, MD 20892

14 edra.london@nih.gov

15 +1 (301) 451-8250

16 Abstract

17

18 The habenula (Hb) is a bilateral, evolutionarily conserved epithalamic structure connecting forebrain and
19 midbrain structures that has gained attention for its roles in depression,¹ addiction,²⁻⁵ rewards
20 processing,⁶ and motivation.^{7,8} Of its two major subdivisions, the medial (MHb) and lateral Hb (LHb),
21 MHb circuitry and function are poorly understood relative to LHb.⁹ *Prkar2a* codes for cAMP-dependent
22 protein kinase (PKA) regulatory subunit II α (RII α), a component of the PKA holoenzyme at the center of
23 one of the major cell-signaling pathways conserved across systems and species. Type 2 regulatory
24 subunits (RII α , RII β) determine the subcellular localization of PKA, and unlike other PKA subunits,
25 *Prkar2a* has minimal brain expression except in the MHb.¹⁰ We previously showed that RII α knockout
26 (RII α KO) mice resist diet-induced obesity (DIO).¹¹ In the present study, we report that RII α KO mice have
27 decreased consumption of palatable, “rewarding” foods and increased motivation for voluntary
28 exercise. *Prkar2a* deficiency led to decreased habenular PKA enzymatic activity and impaired dendritic
29 localization of PKA catalytic subunits in MHb neurons. Re-expression of *Prkar2a* in the Hb rescued this
30 phenotype confirming differential roles for *Prkar2a* in regulating the drives for palatable foods and
31 voluntary exercise. Our findings show that in the MHb decreased PKA signaling and dendritic PKA
32 activity decrease motivation for palatable foods, while enhancing the motivation for exercise, a
33 desirable combination of behaviors.

34 **Introduction**

35

36 In the face of the global obesity epidemic, it remains unclear what makes some individuals more
37 susceptible to obesity than others. Years of cumulative data show that the seemingly simple idea of
38 balancing caloric intake with energy expenditure is complex and influenced by many opposing drives
39 that are exacerbated by overscheduled sedentary lifestyles, changes in the food supply, and genetics.¹²

40 As a major player in the regulation of the midbrain monoaminergic system,⁶ the Hb is a central structure
41 that integrates rewards with cognition and emotion.¹³ While these Hb functions have been investigated
42 in the context of substance abuse, a role for the Hb in obesity and susceptibility to the energy imbalance
43 that drives preventable metabolic dysregulation is less clear.

44

45 To date, MHb research has primarily centered around addiction and mood-related disorders.² The MHb
46 integrates the dysregulated rewards signaling that underlies the imbalance between reward seeking and
47 avoidance behaviors in depression and substance abuse,^{2,14} and it has been suggested that this circuitry
48 may be important to obesity, it has not been systematically investigated. While LHb connectivity and
49 function has been more extensively studied¹⁵ it is increasingly evident that there may be complementary
50 or synergistic roles for the MHb and LHb in regulating stress response, nociception, rewards, locomotor
51 activity and food intake. In the regulation of hedonic eating, the LHb mediates inhibition of palatable
52 food intake through glutamatergic neurons that project from the lateral hypothalamus.¹⁶ Crosstalk
53 between the MHb and LHb is unidirectional from MHb to LHb,¹⁷ and while the interpeduncular nucleus
54 (IPN) is a primary output target of both the LHb and MHb, each innervates distinct IPN structures.^{18,19}

55

56 The MHb is subdivided into dorsal (dMHb) and ventral MHb subnuclei (vMHb), which can be identified
57 by high expression of substance P or acetylcholine, respectively.²⁰⁻²² Developmental elimination of
58 dMHb neurons via deletion of the transcription factor *Pou4f1* blunted sucrose preference,⁸ but a deeper
59 understanding of which cell populations in the MHb can regulate food rewards or signal satiety is
60 lacking. We show here that *Prkar2a*, which codes for the cAMP-dependent protein kinase (PKA)
61 regulatory subunit II α (RII α), is highly expressed in the MHb in a region that overlaps the dMHb and
62 vMHb subnuclei and is therefore present in both acetylcholine- and substance P-expressing cells.

63

64 The few animal studies investigating PKA signaling in the MHb have demonstrated neuroendocrine
65 functions via both pre- and post-synaptic modulation of PKA activity.²³⁻²⁵ In MHb axons, selective
66 inhibition of PKA reversed the induction of glutamate release by atrial natriuretic peptide that plays a
67 role in stress-induced analgesia.²⁵ Additionally, the modulation of local cAMP levels in MHb NACHRs
68 regulates nicotine intake through the diabetes-associated gene, TCF7LR.⁴ These studies provide clear
69 and divergent evidence for regulatory roles for PKA in the Hb, but the breadth of knowledge about
70 specific roles of PKA activity or its inhibition in the MHb is incomplete. In mice, deletion of *Prkar2a* led to
71 a DIO-resistant phenotype and improved glucose tolerance after chronic HFD-feeding.¹¹ There was no
72 detectable metabolic phenotype under normal feeding conditions.^{11,26} The observed DIO-resistance, that
73 was more prominent in female mice, could not be fully explained by altered metabolic rate that was
74 only modestly increased after high-fat diet (HFD) exposure,¹¹ but instead appeared to be the result of
75 decreased HFD intake. Here, we explore how *Prkar2a* might regulate behaviors related to food intake,
76 the motivation for natural rewards, and energy expenditure, and how PKA signaling in the MHb might be
77 altered by the deletion of *Prkar2a*.

78

79 **Results**

80

81 ***Prkar2a* expression is localized to both substance P- and acetylcholine-expressing cells in the MHb**

82

83 Combinations of two PKA catalytic (C α , C β , C γ) and two PKA regulatory (RI α , RI β , RII α , RII β) subunits
84 form the PKA holoenzyme; isoform composition of the tetrameric enzyme is tissue-specific and affects
85 cAMP binding affinity and cellular localization. All subunits except for RII α have high brain expression,
86 yet expression for each appears to be specific,¹⁰ and largely non-redundant. At both RNA and protein
87 levels, RII α was expressed in both the dMHb and vMHb and around the junction of the two subnuclei
88 (Fig 1A). The virtual absence of *Prkar2a* in other brain regions is evident from whole brain view, 3-D *in*
89 *situ* hybridization (ISH) data (Fig 1B, Allen Brain Institutes). Because the habenular structure changes
90 morphologically anterior to posterior, we mapped the expression of *Prkar2a* throughout the Hb from
91 bregma -1.0 mm to -2.0mm and found that *Prkar2a* expression peaked between bregma-1.3– -1.7mm
92 (Suppl Fig 1A). These mapping studies also show that *Prkar2a* expression patterns throughout the dMHb
93 and vMHb vary from anterior to posterior points in the MHb. We used ISH with probes for *Syn-1* and
94 *Gfap* to establish *Prkar2a* expression in both neuronal and glial cells of the MHb (Suppl Fig 1B). Both
95 MHb and LHb neurons use glutamate as their primary neurotransmitter.^{27,28}

96

97 We initially confirmed that *Prkar2a* expression was limited to glutamatergic neurons and not expressed
98 in a subset of GABAergic cells in WT mice by ISH using probes for *Slc17a7* and *Gad1* (Suppl Fig 1C). In line
99 with our expression studies, *Prkar2a* was the only PKA regulatory subunit identified as a highly and
100 differentially expressed gene among the identified cell subsets within the MHb via single-cell

101 transcriptome analysis of mouse.²⁹ High relative expression of *Slc17a6* and *Slc17a7*, that code for
102 vesicular glutamate transporters 1 and 2, and *Tac2* (coding for tachykinin precursor 2) were a common
103 feature among five distinct neuronal cell populations identified in the MHb.²⁹ To characterize the
104 subsets of *Prkar2a*-expressing glutamatergic cells, we performed ISH with probes for *Chat*, *Tac1*, *Tac2*,
105 and *Tac1r*. *Prkar2a* was colocalized with choline acetyltransferase (*Chat*) primarily in vMHb (Figs 1C–D)
106 and with tachykinin precursor 1 (*Tac1*) in the dMHb and to a lesser extent in the vMHb (Fig 1D). *Tac2*
107 was distributed throughout the dMHb and vMHb and was expressed in 65.02 ± 2.20 % of *Prkar2a*-
108 expressing cells (Figs 1E, G). Similarly, *Tac1* was expressed in 46.11 ± 7.26 % *Prkar2a*-expressing cells in
109 the MHb, where these genes are highly and specifically expressed (Figs 1D-E, 1G). *Tac1r* was expressed
110 in 39.99 ± 7.01 % in *Prkar2a*-expressing cells (for which substance P is the substrate) (Fig 1F-G), and *Chat*
111 was expressed in 15.10 ± 1.45 % of the *Prkar2a*-expressing cells (Figs 1C-D, 1G). The colocalization
112 studies showed that *Prkar2a* is expressed in a heterogenous population of MHb cells and is expressed in
113 both substance P- and acetylcholine-producing neurons.

114

115 ***Habenular PKA enzymatic activity is decreased in RllαKO mice***

116

117 In the Hb of RllαKO mice, cAMP-stimulated PKA enzymatic activity was significantly decreased and basal
118 activity tended to be blunted (Fig 2A, left). However, PKA enzymatic activity was unchanged in pre-
119 frontal cortex and striatum, two regions that provide direct input to the Hb (Fig 2A). Thus, disrupted
120 cAMP signaling in the MHb is due to cell-autonomous *Prkar2a* deficiency. Further, the impact on cAMP-
121 stimulated PKA activity suggests a blunted response to upstream signaling events in response to stimuli
122 and not just a generalized decrease in activation under basal conditions.

123

124 Because cells in the vMHb release acetylcholine onto the interpeduncular nucleus (IPN), the primary
125 efferent of the MHb, we measured acetylcholine levels in the IPN. The habenula highly expresses NAChR,
126 subtypes $\alpha 3$, $\beta 3$ and $\beta 4$ and therefore, habenular acetylcholine concentrations were also measured.
127 Acetylcholine concentrations were significantly lower in both the Hb and IPN of RII α KO compared to WT
128 mice (Fig 2B). Additionally, we found comparable levels of glutamate in Hb between genotypes and
129 decreased glutamate concentrations in the IPN in RII α KO mice (Fig 2C). To investigate alterations in the
130 PKA subunit expression in the Hb, we quantified the mRNA and protein levels of the PKA subunits known
131 to compensate for perturbations in the PKA system. mRNA levels of *Prkar1a* and *Prkaca* did not differ in
132 RII α KO Hb compared to WT mice, but RI α protein tended to be lower and C α was significantly reduced
133 in RII α KO Hb lysates (Figs 2D–E). Total PKA catalytic subunit (α , β , and γ) protein levels were also lower
134 in Hb of RII α KO mice (Fig 2E). This is not unexpected as PKA is typically not regulated at the
135 transcriptional level, but is instead regulated via post-translational changes in the stability of the PKA
136 holoenzyme or free catalytic subunit.³⁰

137

138 ***Localization of PKA catalytic subunits to MHb dendrites is disrupted in RII α KO mice***

139

140 Cellular localization of the PKA catalytic subunits and RII α was investigated in the MHb at the point
141 where dMHb and vMHb meet in the center of the structure. Altered subcellular localization of PKA
142 subunits can affect neuronal signaling and impact cellular function and phenotypic characteristics.³¹ PKA
143 catalytic subunits localized to both the cytoplasm and the nucleus within the cell body, and to the
144 dendrites in the MHb of WT mice (Fig 2F, left panel). In RII α KO mice, however, localization of PKA
145 catalytic subunits in dendrites was severely impaired and total catalytic subunit expression appeared to
146 be decreased, a feature that was confirmed quantitatively by western blot (Fig 2F, right panel; Fig 2E). In

147 WT mice, PKA RII α was localized to the cytoplasm as well as to dendrites in MHb neurons, that was
148 absent in RII α KO mice (Fig 2G). MHb excitatory inputs come through the stria medullaris from the
149 septum, nucleus accumbens (NAc) and the cholinergic broca diagonal band,^{13,32,33} and high expression of
150 GABA-B receptors in the MHb^{34,35} suggests strong inhibitory inputs. The diverse connectivity of the MHb
151 demonstrates a clear linkage to rewards circuitry involving both inhibitory and excitatory inputs that
152 could be disrupted by impaired post-synaptic signaling due to PKA deficiency in the MHb.

153

154 ***RII α KO mice have decreased intake of palatable food when provided chronic ad-libitum access***

155

156 To determine whether RII α KO mice consume less palatable HFD when given free access, we provided
157 young adult male and female RII α KO and WT littermate mice with *ad libitum* HFD for 3 weeks. Female
158 RII α KO mice consumed less energy than their WT littermates ($p=0.0091$, two-way ANOVA), a
159 phenomenon not observed in male mice (Fig 3A). Differences between genotypes were greater before
160 adjusting for body weight (data not shown). Binge-eating affects both sexes, but occurs more often in
161 women,³⁶ a sex difference that has been replicated in rodent models.³⁷ Studies with dopamine (DA)
162 antagonists have demonstrated that DA is important for the learned responses to food that relate
163 directly to food reward reinforcement.^{38,39} Removal of HFD after chronic exposure drives dysregulation
164 of DA signaling in female, but not male mice. Interestingly, when exposed to HFD for longer periods of
165 time, a pattern of significantly reduced intake emerged in male RII α KO mice (data not shown).
166 Cumulative energy intake for the 3wk study was significantly higher in female WT compared to KO mice
167 (WT: 13.50 ± 0.51 kcal/g BW and KO: 11.76 ± 0.33 kcal/g BW) and did not differ between males (data not
168 shown). Female RII α KO mice tended to gain less weight during HFD-feeding ($P = 0.059$) (Fig 3B), and
169 metabolic efficiency did not differ significantly from WT littermates (Fig 3C) consistent with our previous

170 indirect calorimetry studies that showed only small difference in resting VO^2 during HFD- but not CD-
171 feeding.¹¹

172

173 Palatable foods are naturally rewarding and their consumption leads to the acute striatal DA release.⁴⁰
174 While striatal PKA enzymatic activity wasn't altered in RII α KO mice on a normal chow diet *in vitro*, HFD
175 increases striatal PKA signaling and alters phosphorylation of DA- and cAMP-regulated phosphoprotein-
176 32 (DARPP-32) in mice.⁴¹ DARPP-32 is a key integrator of DA and glutamate signaling in the basal ganglia
177 that is highly expressed in striatal spiny neurons and can act either as an inhibitor of protein
178 phosphatase 1 or PKA via T³⁴ or T⁷⁵ phosphorylation, respectively.⁴² Based on this and habenular
179 complex connectivity in which the MHb is a central mediator of DA signaling between NAc and VTA,¹³ we
180 investigated striatal phosphorylation of DARPP-32 . We found significant alterations in DARPP-32
181 phosphorylation after chronic HFD- but not CD-feeding in KO compared to WT mice. Phosphorylation of
182 DARPP-32 at Thr³⁴ was decreased in mutant mice after HFD but not CD-feeding compared to WT
183 littermates (Fig 3D; top: CD, bottom: HFD). Phosphorylation of DARPP-32 at Thr⁷⁵ was unchanged in
184 RII α KO mice irrespective of diet (Fig 3D). Striatal sections from WT and RII α KO mice stained for DARPP-
185 32 did not appear to have different cellular distribution of DARPP-32 (Fig 3E). Decreased striatal DARPP-
186 32 has been reported in the Δ FosB mouse, a model of increased reward sensitivity characterized by
187 decreased HFD intake and lower levels of striatal pCREB.⁴³ Our results suggest that blunted striatal
188 DARPP-32 T³⁴ phosphorylation is associated with decreased intake of HFD in RII α KO mice. Rodent
189 studies have shown that chronic HFD causes changes in the DA signaling system, including lower basal
190 DA levels in the NAc.^{40,44} Furthermore, acute or chronic treatment with the selective serotonin reuptake
191 inhibitor, fluoxetine led to increased phosphorylation of DARPP-32 at Thr³⁴ and decreased
192 phosphorylation at Thr⁷⁵ in striatum.⁴⁵ Here we show differences in striatal DARPP-32 phosphorylation

193 in RII α KO mice after 3wk HFD feeding and decreased intake among mutant females and males (over a
194 longer period of HFD exposure).

195

196 ***Fasted RIIAKO mice have decreased drive for food reward***

197

198 RII α KO and WT littermates trained to perform an operant lever press task on a fixed ratio schedule of
199 food pellet delivery were then subjected to a progressive ratio operant task in both the fed and fasted
200 states. There were no differences in learning the operant task as assessed by percent correct and
201 incorrect lever presses and in achieving the goal of earning 50 food pellets with at least 80% correct
202 lever presses (data not shown). Additionally, the amount of time spent engaged in the operant task and
203 the drive to work for food reward assessed (i.e., breakpoint) in non-fasted mice did not differ between
204 genotypes (Figs 4A-C). After a 14h overnight fast, RII α KO mice spent less time engaged in the
205 progressive ratio task (Fig 4A), had a lower breakpoint and earned fewer food reward pellets than their
206 WT littermates (Figs 4B-C).

207

208 ***RIIAKO mice drink less sucrose solution and have blunted sucrose preference***

209

210 To further evaluate the role of *Prkar2a* in hedonic drive for natural rewards, we performed sucrose
211 preference tests in male and female mice using 10% (wt/vol) sucrose solution and a standard two-bottle
212 paradigm. Sucrose preference is a well-established test for anhedonia, defined as the lack of ability to
213 experience pleasure from rewarding or enjoyable activities.⁴⁶ When given 24h access to both 10%
214 sucrose and water for 3 consecutive days per week over a 2-week period, multiple comparisons

215 revealed similar sucrose intakes between WT and RIIAKO mice on day 1, but RIIAKO mice had lower
216 intake levels than WT mice on subsequent days (Fig 4D). There was a significant genotype effect on
217 sucrose intake for female and male mice ($P = 0.0095$, $P = 0.0053$, two-way ANOVA). Similarly, after the
218 initial 24h period, sucrose preference was significantly decreased in male RIIAKO mice ($P = 0.0073$),
219 highlighting a sex difference in the *Prkar2a*-mediated regulation of sucrose reward (Fig 4E).

220

221 Despite the lack of differences in energy intake from chow between genotypes (data not shown), male
222 RIIAKO mice had decreased total energy intake due to differences in sucrose consumption and gained
223 less weight than WT littermates during the 2wk experiment (Figs 4F-G). There were no differences in
224 cumulative total energy intake or weight gain after sucrose access in female mice (Figs 4F-G).

225

226 Circuits between the lateral hypothalamus and the VTA, an indirect target of the MHb, play a role in
227 sucrose seeking and reward encoding,⁴⁷ and tachykinins (derived from the MHb) are involved in umami
228 and perhaps other taste modalities.⁴⁸ VTA glutamate neurons have also been associated with positive
229 reinforcement during reward-based operant tasks mediated by their release of GABA.⁴⁹ Thus, disruption
230 of these signals through decreased MHb signaling to the VTA via the IPN may act to impair reward
231 processing and reinforcement.

232

233 ***RIIAKO mice have increased drive for voluntary running***

234 Motivation for exercise can play an important role in energy homeostasis and this drive is regulated by
235 shared circuitry that regulates other natural rewards yet has distinctions from those mediating food
236 reward (i.e., taste vs locomotor activity). The Hb plays a role in regulating the temporal pattern of

237 locomotor activity throughout the night.⁵⁰ Moreover, both developmental ablation of dMHb neurons, or
238 maturation defects in the MHb severely impair voluntary wheel running behavior in mice.^{7,8} Thus, we
239 investigated voluntary exercise performance of RII α KO mice. When provided with home cage running
240 wheels, RII α KO mice ran 2-3 times the distance than that of their WT littermates (Fig 5A-B). *Prkar2a*
241 heterozygosity rescued the high running phenotype of RII α KO mice to levels of WT mice. These data
242 suggest that even partial restoration of RII α -mediated PKA activity and holoenzyme localization suffices
243 to reverse the change in PKA signaling responsible for the observed motivation for running. Total wheel
244 turns for the 2-week running experiment was significantly lower for both WT and RII α +/- mice compared
245 to RII α KO mice for both sexes (Fig 5A-B). The timing of running activity across light:dark cycles and
246 within the active dark cycle was as expected with spikes of activity in the early dark period and tapered
247 activity in the later part of the dark cycle and did not differ among genotypes. We previously showed
248 that normal home cage locomotor activity was not different between WT and RII α KO mice of either
249 sex.¹¹ Denial of the expected access to running wheels was identified as activating striatum, lateral
250 hypothalamus and frontal cortex in mice selectively bred for running, suggesting that omission of
251 reward led to anxiety or stress.⁵¹

252

253 Given the increased motivation for running in RII α KO mice, we hypothesized that mutant mice
254 accustomed to daily wheel running might experience stress that could be detected by Hb activation in
255 the absence of this natural reward. The MHb was identified as one of six limbic regions that are
256 susceptible to stress-induced c-Fos expression⁵² and c-Fos was identified in MHb and LHb in response to
257 restraint stress and forced swim test.⁵³ Therefore, we decided to assess both c-Fos and c-Jun expression
258 in response to being blocked from the expected running wheel access. In RII α KO mice, blocking access to
259 running wheels prior to onset of the dark cycle resulted in increased c-Fos and c-Jun expression in the
260 MHb (Figs 5D-E). Induction of c-Fos and c-Jun was not observed in the MHb of WT mice that were

261 blocked from running. Regardless of genotype, no immediate early gene (IEG) induction in the Hb was
262 observed in mice that had continued access to running wheels (Fig 5D, right panels), suggesting that
263 hyperactivation of the MHb may be associated with stress or anxiety related to withholding the
264 pleasurable experience of running. Additionally, when similar studies were conducted after mice were
265 habituated to sucrose access, no IEG induction was observed in WT or KO mice under either reward or
266 blocked reward conditions (data not shown).

267

268 ***rAAV-mediated habenular Prkar2a re-expression rescues sucrose preference and running phenotypes***

269

270 We hypothesized that the behavioral phenotypes observed were driven specifically by *Prkar2a* deletion
271 in the Hb. We delivered a recombinant adeno-associated viral (rAAV) vector with a construct containing
272 *Prkar2a* and GFP via bilateral stereotaxic injections to young adult WT and RII α KO mice (both sexes) (Fig
273 6A). Pilot injections first with retrobeads and then with a GFP-containing rAAV were used to confirm
274 injection coordinates. Post-experimental injection accuracy was confirmed by immunofluorescence for
275 each mouse (Suppl Fig 2; Fig 6B is a representative image of the expected re-expression of PKA RII α).
276 RII α KO mice with off-target injections were classified by lack of immunofluorescent signal for RII α and
277 GFP in the MHb and subsequently excluded from the data analysis. Two to 3-weeks after a surgery, a
278 period that was sufficient for recovery, and to ensure adequate RII α protein expression, sucrose
279 preference tests were performed followed by a 2-week washout period prior to initiating 2-week
280 running wheel experiments. Re-expression of *Prkar2a* in the MHb rescued the sucrose intake and
281 preference phenotype of RII α KO mice (Fig 6C) as well as the increased voluntary running phenotype (Fig
282 6D). There were no differences between mean sucrose intake or preference levels or of total wheel

283 turns in the rAAV-injected WT or rAAV-injected RII α KO mice, confirming that habenular *Prkar2a*
284 inversely regulates voluntary exercise and sweet reward responses.

285

286

287 **Discussion**

288

289

290 Across species, a positive response to natural rewards is an innate survival mechanism that is driven by
291 the cognitive processing of pleasure experienced from activities like eating, running (as prey or
292 predator), or sex. While being able to experience the rewarding aspects of food is evolutionarily vital,
293 overriding satiety signals in favor of the overconsumption of high-fat and sweet foods can lead to
294 obesity, metabolic dysregulation, and other related comorbidities. Achieving weight loss and
295 maintaining energy balance by moderating food intake and increasing physical activity underlies the
296 battle against dietary obesity and weight gain. The habenula is central to reward and aversion systems
297 which are both necessary for maintaining balance in processing rewards stimuli. The LHb is critical in
298 transmitting negative-reward signals and a rewarding stimuli causes decreased LHb activity in concert
299 with increased DA activity, while the reverse is true of punishing stimuli.^{6,54} While, the habenula has
300 been hypothesized to serve as nexus of the complex reward circuitry with a key role in maintaining the
301 balance between reward-seeking and avoidance behaviors,² much less is known about the roles for the
302 MHb in these processes.

303

304 Here we identify an unexpected role for PKA RII α in the MHb in the simultaneous positive regulation of
305 food rewards and negative effect on the drive to exercise, behaviors that were both reversed with RII α

306 deficiency. The diminishment of both drives is characteristic of the anhedonia observed in major
307 depressive disorder (MDD),⁵⁵ and LHb hyperactivation has been associated with both the
308 neurobiological dysregulation and the motivational symptoms of depression.⁵⁶ We demonstrate a
309 significant decrease in cAMP-stimulated PKA activity as well as altered dendritic localization of “active”
310 free PKA catalytic subunits in MHb of the RII α KO mouse. Given the direct and unidirectional input from
311 the MHb to LHb,¹⁷ it seems likely that input to the LHb is likely also impacted by the altered MHb PKA
312 signaling in RII α KO mice. Decreased LHb activity inversely impacts local DA activity that has downstream
313 effects on VTA, a pathway that has notable overlap with the VTA-lateral hypothalamus-NAc pathway.
314 Impaired DA signaling is a common thread that connects compulsive behaviors related to food intake,
315 substance abuse and the motivation symptoms of depressive disorders. In both obesity and substance
316 abuse, the dysregulation of DA signaling and subsequent changes in reward circuitry can fuel the cycle of
317 compulsive drug or compulsive food consumption.

318

319 Altered DA signaling downstream of MHb after chronic HFD exposure was evidenced in the RII α KO
320 mouse by decreased striatal DARPP-32 T³⁴ phosphorylation (Fig 3D). In intact neurons, T³⁴
321 phosphorylation inhibits protein phosphatase 1, that in turn inhibits D₁ DA signaling.⁴² After roux-en-Y
322 gastric bypass, mice had increased DA D1R activity and reduced fat intake via PPAR α -vagal-D1R
323 signaling, unlike sham operated mice.⁵⁷ Additionally, studies in the Δ Fos-overexpressing mouse, a model
324 of increased reward sensitivity confirm the importance NAc feedback to the VTA in regulating DA
325 signaling and moderating HFD intake. While chronic HFD led to decreased mRNA expression of tyrosine
326 hydroxylase and DA transporter in VTA of control mice, levels of both were increased in the reward-
327 sensitive Δ Fos mouse.⁴³

328

329 Blunted sucrose intake was a clear phenotypic characteristic of mice lacking *Prkar2a* and was strongest
330 in males (Fig 4D-E). Whereas sucrose intake escalated in WT mice after its introduction and a high level
331 of daily sucrose intake was maintained, the intake pattern for RII α KO mice suggests decreased
332 motivation and altered reward processing. It is important to note that RII α KO mice prefer both HFD and
333 sucrose solution when offered the choice between normal chow or HFD and 10% sucrose or water,
334 respectively. The significant decrease in breakpoint, time engaged in the task, and number of rewards
335 earned during operant progressive ratio tasks in fasted RII α KO compared to WT mice further suggests
336 the presence of an intact reward circuit, but decreased appetitive motivation that could lead to the
337 “moderation” phenotype seen in RII α KO mice with respect to palatable foods.

338

339 Sucrose preference and the behavioral and physiologic responses to chronic HFD exposure were sex-
340 dependent in RII α KO mice. Our observations with regards to sex differences in the recorded behaviors
341 and metabolic parameters are consistent with other mouse models of PKA deficiency or
342 overexpression, in which sexual dimorphism is a common characteristic.⁵⁸ While the requirement to
343 include females in clinical and basic research protocols is relatively recent, mounting evidence suggests
344 key differences in the regulation of behaviors linked to DA (and other monoamine) signaling. We report
345 a more pronounced decrease in sucrose intake and preference in male compared to female RII α KO
346 mice, while decreases in intake, weight gain and metabolic efficiency during chronic HFD feeding were
347 significant only in female KO mice. Clinical studies of depressive disorders reinforce key differences in
348 the prevalence of depression and the response to anti-depressant drugs between sexes.⁵⁹ Binge-eating
349 is more frequent in women,³⁶ a findings that is replicated in rodents.³⁷ Thus the inhibition of HFD intake
350 in female mice via *Prkar2a* deletion is particularly interesting. Additionally, depression is more prevalent
351 in females,⁶⁰ who are also significantly more sensitive to the anti-depressive effects of ketamine⁶¹ and
352 traditional SSRI anti-depression drugs via an ovarian hormone dependent mechanism.⁶¹ In MDD, women

353 experience greater anxiety and somatic symptoms that include disturbances in sleep, appetite and
354 pain.⁶² Sex-dependent mid-brain monoamine regulation likely underlies a number of signaling processes
355 involved in mood, intake of palatable foods and the pleasure derived from naturally rewarding
356 behaviors including those observed in the RII α KO mouse. Further interrogation of behavior and
357 physiologic responses to both rewarding and aversive stimuli in male and female RII α KO mice may
358 provide deeper insight into the mechanisms that underly the observed differences. Our data show that
359 comparable reductions in Hb PKA activity and neurotransmitter levels in Hb and IPN in male and female
360 mice elicit distinct effects in reward signals that can impact intake and body weight.

361

362 The dysregulated PKA signaling induced via *Prkar2a* deletion in the MHb causes decreased acetylcholine
363 release in both the Hb and the IPN, as well as decreased glutamate levels in the IPN (Figs 2B-C). Hb
364 acetylcholine signaling has been linked to both nicotine addiction and the aversive aspects of
365 withdrawal,⁶³ depressive disorders,⁶⁴ and more recently nicotine addiction has been linked to impaired
366 glucose control via Hb-gut connections.⁴ While downregulation of cholinergic signaling caused
367 anhedonia-like behavior but not despair,⁶⁴ the developmental ablation of MHb neurons using a *Pou4f-*
368 cre driver in mice blunted both voluntary exercise and sucrose drinking, without other depression-
369 related symptoms.⁸ Here we show that impaired *Prkar2a* regulation of PKA activity in MHb clearly
370 enhances the drive for voluntary exercise that could occur by altered localization of active PKA or
371 decreased total activity. However, the previously described mouse models and disease states such as
372 MDD and other depressive disorders, obesity, and in the first two of the three stages of the drug
373 addiction cycle (intake/binge, aversive cycles),⁶⁵ involve the regulation of these drives in the same
374 direction. *Prkar2a* is expressed in heterogenous cell populations within the dMHb and vMHb, in both
375 substance P- and acetylcholine-expressing cells and is expressed in glia and neurons which likely explains
376 the differential regulation of exercise and food reward drives. We have shown the direct impact of

377 *Prkar2a* deletion on acetylcholine and glutamate levels. *Prkar2a* is also highly expressed in *Tac1*- and
378 *Tac2*-expressing cells of the MHb and thus, further study of PKA regulation in the various distinct cell
379 subtypes is warranted.

380

381 Apart from what was learned from studies in the Δ Fos-overexpression and *Pou4f*-cre driven MHb
382 neuronal ablation mouse models, the RII α KO mouse implicates the downregulation of PKA activity in
383 MHb in the regulation of two overlapping but distinct pathways. Re-expression of *Prkar2a* in Hb of the
384 global RII α KO mouse rescued the sucrose and running phenotypes confirming that both behaviors are
385 mediated by changes in habenular PKA signaling. Whereas the observed blunted response to sucrose
386 and HFD and the decreased appetitive drive to obtain food rewards in the fasted state resemble
387 anhedonia-like behaviors associated with MDD, the decreased locomotor typically observed with
388 anhedonia is absent in this mouse model. While the connections to food reward behaviors in the RII α KO
389 mouse are clearer, the link to enhanced voluntary activity seems more complicated despite the known
390 relationship between reward seeking and locomotor sensitization.⁶⁶ The inverse regulation of
391 consummatory drive and the drive to engage in exercise caused by *Prkar2a* deficiency generates a
392 desirable phenotype of sucrose and HFD intake moderation and of enhanced motivation for exercise.
393 We identify habenular *Prkar2a* as a new player in regulating the habenular complex (aka, dorsal
394 diencephalic conduction system), and provide new insights into the role of habenular PKA signaling, the
395 regulation of hedonic drive and susceptibility to dietary obesity.

396 **Methods**

397

398 *Mice.* RII α KO mice were obtained from MMRRC and have previously been described.²⁶ RII α
399 heterozygous breeding pairs were bred on a C57/Bl6 background to generate WT and KO littermates.
400 This mouse line has been bred in our mouse facilities for approximately 10 years which ensures >99%
401 C57/Bl6 background. A standard 0600h:1800h light/dark cycle was consistently maintained with an
402 average temperature of 73°F. Mice were all handled regularly by the same individuals for the at least 2-3
403 weeks leading up the behavioral studies.

404

405 *Ad libitum HFD feeding studies.* To measure intake of palatable chow we used Bio-Serv #F3282, soft
406 high-fat diet (HFD) that provides 5.49 kcal/g and derives approximately 15%, 59% and 26% of total
407 energy from protein, fat and carbohydrate, respectively. Young adult (12–16-week old) male and female
408 WT and RII α KO littermates were individually housed and provided free access to drinking water and
409 HFD. Body weight and weight of the food consumed were measured weekly for 3 weeks. Mice were
410 maintained on the same 12h light:dark cycle and temperature and humidity conditions that they had
411 been acclimated to from birth.

412

413 *Sucrose intake and sucrose preference test.* Sucrose preference was evaluated in individually housed WT
414 and RII α KO littermates by providing identical bottles containing water and 10% (w/v) sucrose solution
415 side by side daily for three consecutive days a week for two weeks. The position of sucrose and water
416 were alternated daily, and the amounts of sucrose solution and water consumed were determined by
417 weighing each bottle when removed from the cage, and for sucrose solution, before replacement with

418 fresh solution. Absolute sucrose solution, water and control chow (CD) (NIH-31) intakes were analyzed,
419 and sucrose preference was calculated as a percent (preference= sucrose solution intake (g) / (water
420 intake (g) + sucrose solution intake (g)) *100.

421

422 *Operant conditioning positive reinforcement studies.* Young adult mice (3-6 months old) were
423 individually housed in cages with a divider and calorie restricted for 1 week to achieve 90% of initial
424 body weight and maintained on an 85% calorie restricted diet for the initial conditioning phase. Briefly,
425 85% of ad libitum intake was determined based on the average daily intake for 3 days. Once 90% of
426 starting body weight was achieved, body weight was monitored daily and caloric restriction continued
427 with adjustments made as needed to ensure optimal weight throughout the training phase. Purified
428 Rodent Dustless Precision Pellets (14 mg, Bio-Serv) were used as food rewards.

429

430 Mice were randomly assigned to either right or left lever press and were trained with a fixed ratio 1
431 (FR1) schedule in which one food pellet was delivered for each correct lever press. The criteria for
432 successful completion of the FR1 and FR5 tasks was receiving 50 food pellets with $\geq 80\%$ correct lever
433 presses within the 60-minute test period. Upon successful completion of the FR1 task for two
434 consecutive days, mice progressed to the FR5 schedule and then to the progressive ratio (PR). Ad libitum
435 feeding was reintroduced for FR5 and PR portions of the study.

436

437 *Voluntary running behavior and blocked running wheel experiments.* Individually housed young adult
438 mice (3-6 months old) were provided with home cage running wheels for two weeks (Med Associates
439 Inc, Fairfax VT). Daily running and total wheel turns were analyzed as 30-minute bins for the entire two-

440 week period. To test the effects of blocking the anticipated natural reward of running on immediate
441 early gene (IEG) expression in habenula we used mice that had been provided free access to home cage
442 running wheels for 2 weeks prior (n=4-6/group). Running wheels were locked but left inside of home
443 cages 2h prior to the onset of the dark cycle (1600h). Between 1.5-2.5h post dark cycle onset, when
444 running levels are typically high (1930-2030h), mice were transcardially perfused and brains harvested
445 and processed as later described for immunofluorescent staining for c-Fos and c-Jun.

446

447 *Dissection of brain for PKA enzymatic activity, ELISA, and western blot.* Brains were cut into 150–200 μ M
448 thick sections and kept cold while dissected using a microscope (SMZ 1500, Nikon). Prefrontal cortex,
449 striatum and habenula were dissected based on stereotaxic coordinates using the following landmarks:
450 prefrontal cortex (bregma 3.0–2.5 mm), bilateral samples taken just above and excluding the orbital
451 area; striatum (bregma 1.5– 0.2 mm), bilateral samples below and on the interior side of the genu of
452 the corpus callosum and along the exterior edge of the lateral ventricle; habenula (bregma -1.0– -2.0
453 mm), bilateral samples taken directly adjacent to third ventricle just below the stria medullaris and
454 above the paraventricular nucleus of the thalamus; interpeduncular nucleus (IPN) (bregma -3.35– -3.45
455 mm) was taken from either side of the midline just dorsal to the middle cerebellar peduncle and ventral
456 to the ventral tegmental decussation, based on *The Mouse Brain in Stereotaxic Coordinates* (Franklin &
457 Paxinos).⁶⁷ Dissected samples were immediately snap frozen in liquid nitrogen and stored at -80°C until
458 assay.

459

460 *PKA enzymatic activity assay.* Tissues were homogenized in freshly prepared lysis buffer (10 mM Tris-HCl
461 (pH 7.5), 1 mM EDTA, and 1 mM dithiothreitol with 0.5 mM PMSF and protease inhibitor cocktail I
462 (1:100; EMD Biosciences, La Jolla CA). BCA assays were performed as per manufacturer's protocol to

463 determine the total protein concentrations of samples (Pierce). Samples were diluted to 1 µg/µL and 10
464 µL of total protein was used for each reaction. PKA enzymatic assays were performed by kemptide
465 assay, using 25 µM kemptide (Leu-Arg-Arg-Ala-Ser-Leu-Gly), as previously described with and without
466 cAMP (5 µM).⁶⁸ All reactions for basal and cAMP-stimulated (total) PKA activity were carried out in
467 duplicate. Additionally, activity values for replicate reactions that were incubated in the presence of PKI
468 (5 nM) were subtracted from activity values to account for non-specific kinase activity.

469

470 *Quantification of acetylcholine.* IPN acetylcholine concentrations were determined by
471 choline/acetylcholine assay kit (Abcam, cat# ab65345) as per manufacturers protocol. Samples were
472 weighed prior to homogenization to standardize the total amount of tissue analyzed. Tissues had been
473 previously snap frozen after micro-dissection from 150-200 µM thick sections at bregma -3.45– -3.5 mm
474 as previously described. After snap freezing, samples were stored at -80°C.

475

476 *Western blotting.* Habenular and striatal lysates were prepared as described for PKA enzymatic activity
477 assays. 10 µg of total protein per lane was loaded onto 4–12% Bis-Tris gels (Bolt Plus, Invitrogen) and
478 run for 35 min at 165 V. For each gel, 7 µL of WesternSure pre-stained protein ladder was loaded onto a
479 separate lane (Li-Cor). Protein was transferred onto nitrocellulose membranes using a semi-dry
480 apparatus for 30 min (TransBlot Turbo, BioRad), stained with Ponceau S stain, washed with 1X TBS with
481 0.1% Tween-20 (1X TBST) and then blocked with 5% nonfat dry milk or bovine serum albumin in 1X TBST
482 for 1 h at room temperature. Membranes were then probed overnight with primary antibodies with
483 gentle shaking at 4°C before washing 3 times with 1X TBST and probing for 1 h at room temperature
484 with the appropriate antibody and Precision Protein StrepTactin-HRP Conjugate (1:10,000, BioRad). All

485 western blots were visualized using either Pierce enzyme chemiluminescent substrate (Pierce) and a
486 ChemDoc analyzer (BioRad). See Supplemental Table 1 for antibodies used, sources and dilutions used.

487

488 *RNA extraction and relative mRNA expression analysis.* RNA was extracted from previously snap frozen
489 Hb that had been stored at -80°C. RNA was extracted by adding 500uL Trizol (Invitrogen) to each sample
490 in a microcentrifuge tube pre-loaded with RNase free beads and homogenized using a Bead Ruptor Elite
491 (Omni International) for 2 X 20 seconds at a speed of 2.4. Samples were centrifuged for 5 minutes at
492 12,000 x g at 4°C. Supernatant was transferred to a clean tube for each sample and incubated for 5
493 minutes before adding 100 µL of chloroform, shaking by hand for 30 seconds and incubating for an
494 additional 3 minutes. Samples were centrifuged for 15 minutes at 12,000 x g at 4°C. The aqueous phase
495 was carefully removed and RNA quantified by nanodrop. 500 ng of total RNA was used to make cDNA
496 for each sample using SuperScript III First Strand Synthesis Supermix for qRT-PCR per manufacturer's
497 protocol (Invitrogen). Quantitative reverse transcriptase polymerase chain reaction (qRT-PCR) was
498 performed on a VIIA7 instrument (BioRad) using a standard 40 cycle program that included melt curve
499 analysis. To determine relative mRNA expression levels of PKA subunits in habenula, the following
500 specific, pre-optimized primers were used (*Prkar1a*: FW 5'-CGAAGAATCCTCATGGGAAG-3', REV 5'-
501 CTCTCCTTGCACCACGATCT-3' ; *Prkaca*: FW 5'-GAAAATCGTCTCTGGGAAGGT-3', REV 5'-
502 TGGCAATCCAGTCAGTCGT-3; *Rplp0*: FW 5'- GAAAATCTCCAGAGGCACCA-3', REV 5'-
503 ACCCTCCAGAAAGCGAGAGT-3'; *18S*: FW 5'-GCAATTATCCCCATGAACG-3', REV 5'-
504 GGCCTCACTAAACCATCCAA-3'. Syber Green *Power* mastermix (10 uL), 1uL of cDNA, 8.4 uL H₂O and 0.3 uL
505 of each primer (10 µM) were combined for each reaction well and each reaction was performed in
506 triplicate (Applied Biosystems, VIIA7). Relative expression was determined using the $2^{-\Delta\Delta CT}$ values that
507 were calculated based on the average CT values for the housekeeper genes determined to be optimal

508 for the sample type (*18S* and *Rplp0*) and values were analyzed as the fold-change from WT values.⁶⁹

509 Melt curves and gel electrophoresis were used to confirm the expected pcr products.

510

511 *Immunofluorescence.* Mice were killed by slow replacement of air with CO₂ (flow rate ≤ 5L/min) followed
512 by cervical dislocation. Mice were transcardially perfused with ice cold 1X PBS (10mL), followed by 4%
513 paraformaldehyde (PFA) (20mL). Whole brains were post-fixed for 1h in 4% PFA, washed 3X with 1X PBS,
514 then cryopreserved in 30% sucrose until brains sunk. Brains were washed again 3X with 1X PBS, and
515 snap frozen in -80°C 2-methylbutane. Floating sections (35µM) were blocked with 5% donkey serum in
516 1X PBS with 0.1% Triton-X 100 and 0.1% glycine for 1h. Sections were incubated with primary antibodies
517 overnight at 4°C with gentle shaking, then washed 3X with 1X PBS with 0.1% Triton-X 100 and then
518 incubated with appropriate secondary antibodies for 1h at 4°C with gentle shaking. Sections were then
519 washed 3X with 1X PBS with 0.1% Triton-X 100 and counterstained with DAPI (1:1000; Sigma Alrich).
520 Antibodies were diluted in 2X diluted blocking buffer. See Supplementary Table 1 for antibodies and
521 conditions used.

522

523 *RNA in situ hybridization.* Brains harvested from RllαKO and WT littermates were immediately snap
524 frozen in isopentane and stored at -80°C until cryo-sectioning. Brains were equilibrated at -20°C for at
525 least 1h prior to sectioning (20 µM thick) on a cryostat (Leica) and mounted directly onto Superfrost
526 slides (Fisher Scientific). Slides were sealed in an airtight bag and stored at -80°C and then fixed in ice
527 cold 4% PFA for 1h at 4°C prior to use. After fixation, slides were dipped in ice-cold 1X PBS, and then
528 dehydrated in an ethanol gradient from 50% to 100% for 5 minutes at each step. Slides were stored in
529 fresh 100% ethanol for up to 7 days at -20°C prior to hybridization. *In situ* hybridization was performed
530 by first pre-treating sections with a RNAScope protease inhibitor IV for 20 minutes and then probed

531 using specific probes (Suppl Table 2) and counterstained with DAPI following the manufacturer's
532 protocol (RNAScope, ACD Bioscience).

533

534 *Fluorescent microscopy.* For *in situ* hybridization expression studies, immunofluorescence experiments
535 and cellular localization studies, images were captured using a confocal microscope with fluorescent
536 filters while maintaining uniform exposure settings across samples within each experimental batch
537 (Zeiss LS800, Germany). A magnification of either 20X (for cell counting and *Prkar2a* colocalization with
538 markers) or 63X with oil (dendrite localization) was used.

539

540 *Quantification of colocalization of Prkar2a with MHb markers.* Colocalization analyses were done using
541 the Zen Blue software (Zeiss LS800, Germany). Sections were probed for *Prkar2a* and one to two other
542 markers of MHb cell subtypes including *Tac1*, *Tac1R*, *Tac2*, *Slc17a7*, and *Chat*, and then counterstained
543 with DAPI. Zen Blue software was used to perform the particle and density analyses (Zeiss, Germany).
544 The polygon drawing tool was used to outline the MHb as the area of interest. The colocalization tool
545 was used as per the manufacturer recommended procedure to determine colocalization between
546 *Prkar2a* and another marker and is widely used for such quantifications (Everett, M. Acquiring and
547 Analyzing Data for Colocalization Experiments in AIM or ZEN Software).⁷⁰ Colocalization thresholds were
548 kept constant within each brain section. The utilized data point was the colocalization coefficient 1:
549 Rhoda-T3, which describes the ratio of colocalized points for *Prkar2a* and the targeted marker to total
550 *Prkar2a* points in the selected area.

551

552 *c-Fos- and c-Jun-positive cell counting.* *c-Fos* or *c-Jun* stained brain sections from mice that were either
553 blocked from or permitted to continue running as previously described were imaged with a confocal
554 microscope using uniform settings (Zeiss LS800) and analyzed using ImageJ software (NIH, Bethesda).
555 The color channels for each image were split apart. Analyses were conducted solely on the red channel
556 image. An outline of the MHb was created using the polygon drawing tool. Image threshold was set to
557 allow for analysis of only legitimate signal. Threshold settings were kept uniform throughout the analysis
558 of each sample. Amount of image particles was obtained using the 'Analyze Particles' function. Particle
559 density ratio was calculated by the equation: (number of particles /area ratio of the MHb), the latter
560 defined as the area of the MHb over the total image area. Area measurements were obtained using the
561 'Measure' function.

562

563 *rAAV-mediated re-expression of Prkar2a.* The construct, pAV-EF1a-mPrkar2a-IRES-eGFP, was generated
564 and packaged into an adeno-associated virus (serotype AAV8) (titer: 1.44×10^{13} GC/mL) (Vigene Bio,
565 Rockville MD) (Figure 6). For construct validation, the vector was transfected into Hek293 cells
566 (Transfectamine 2000, Invitrogen), and cells were lysed at 48h post-transfection to confirm expression
567 of *Prkar2a* and GFP gene products. Survival surgery was performed on male and female RII α KO and WT
568 mice (n=9-11/genotype) using aseptic techniques. Mice were anesthetized with 5% isoflurane and
569 mounted on a stereotaxic frame with an integrated a computer atlas (Leica Angle Two) to aid with
570 injection angles. Topical lidocaine/prilocaine cream (2.5%/2.5%) and buprenorphine (0.1 mg/kg via
571 subcutaneous injection) were administered for post-operative analgesia. Following midline incision, 1
572 mm holes were drilled bilaterally at the following injection sites: anterior/posterior: -1.53 mm from
573 bregma, lateral: (-/+) 0.17 mm, depth: -2.5 mm. A glass micropipette was used to deliver a volume of
574 100 nL of rAAV at a flow rate of 0.1 μ L/min at 10.08° angles. Retrobeads (Lumafluor) were used initially
575 to confirm the injection coordinates. Mice were provided with topical lidocaine/antibiotic ointment and

576 ketoprofen daily for at least 3 days following surgery and were observed regularly during the two-week
577 recovery period that also enabled expression of the target proteins prior to behavior testing. Upon
578 completion of post-rAAV injection behavior testing, mice were sacrificed and perfused, and brains
579 prepared for immunofluorescence as described below. rAAV-injections were validated by fluorescent
580 microscopy targeted to habenula and surrounding areas (Keyence, Japan) (Suppl Fig 2). RII α KO and WT
581 mice in which habenular expression of GFP and RII α expression was not achieved were excluded from
582 the experimental data.

583

584 *Statistics.* GraphPad Prism version 8.4.2 was used for all statistical analyses. Alpha was set at 0.05 and a
585 *P* value of < 0.05 was considered as significant. When applicable, two-way unpaired t-test were used to
586 compare WT and RII α KO mouse data when normality assumptions were met. For data that were not
587 normally distributed, the Mann Whitney rank test was used. For data sets including multiple time points,
588 repeated measures two-way ANOVA analysis was used to evaluate the effect of genotype and of
589 genotype and time on intake levels and preference. The Geisser-Greenhouse correction was used as
590 needed to correct for unequal variability of differences. Multiple comparisons for one-way and two-way
591 ANOVA analyses were done using Bonferroni's post hoc test to compare individual mean values for HFD
592 intake, sucrose intake and preference between genotypes. Two-way unpaired t-tests were used for data
593 that were normally distributed and the Mann-Whitney rank test were applied to data that did not meet
594 the normality assumptions. Tests used and *P* value ranges are detailed in the figure legends.

595

596 *Study approval.* All procedures were carried out in accordance with the National Institute of Child Health
597 and Human Development Animal Care and Use Committee guidelines.

598

599 Acknowledgements: Funding by the *Eunice Kennedy Shriver* National Institute of Child Health and
600 Human Development Division of Intramural Research. We would like to thank Daniel Abebe for his
601 invaluable help in setting up the murine behavior testing and Oksana Gavrilova for her guidance on
602 phenotyping and thought provoking discussions about experimental design.

603

604 Author contributions: Edra London designed and conducted the mouse behavioral studies, the
605 biochemical, histological, and molecular biology experiments and microscopy; managed data and data
606 analysis and statistics and prepared the manuscript. Jason Wester designed, optimized, and performed
607 all stereotaxic surgeries, provided guidance on data presentation and analyses, and contributed to the
608 manuscript preparation. Michelle Bloyd conducted the mouse behavioral studies, optimized
609 methodologies for analyzing the Prkar2a localization and IEG cell counting data, assisted with sample
610 preparation, and manuscript preparation. Shelby Bettencourt conducted the mouse behavioral studies
611 and assisted with the related data compilation and analyses, sample preparation and contributed to the
612 preparation of the manuscript. Chris McBain provided input regarding experimental design and data
613 analyses and contributed to manuscript preparation. Constantine Stratakis contributed to the project
614 and experimental design, data analyses and manuscript preparation.

615 1 Hikosaka, O. The habenula: from stress evasion to value-based decision-making. *Nat Rev*
616 *Neurosci* **11**, 503-513, doi:10.1038/nrn2866 (2010).

617 2 Mathis, V. & Kenny, P. J. From controlled to compulsive drug-taking: The role of the habenula in
618 addiction. *Neurosci Biobehav Rev* **106**, 102-111, doi:10.1016/j.neubiorev.2018.06.018 (2019).

619 3 Mathieu-Kia, A. M., Pages, C. & Besson, M. J. Inducibility of c-Fos protein in visuo-motor system
620 and limbic structures after acute and repeated administration of nicotine in the rat. *Synapse* **29**,
621 343-354, doi:10.1002/(sici)1098-2396(199808)29:4<343::aid-syn6>3.0.co;2-5 (1998).

622 4 Duncan, A. *et al.* Habenular TCF7L2 links nicotine addiction to diabetes. *Nature* **574**, 372-377,
623 doi:10.1038/s41586-019-1653-x (2019).

624 5 Antolin-Fontes, B. *et al.* The habenular G-protein-coupled receptor 151 regulates synaptic
625 plasticity and nicotine intake. *Proc Natl Acad Sci U S A* **117**, 5502-5509,
626 doi:10.1073/pnas.1916132117 (2020).

627 6 Matsumoto, M. & Hikosaka, O. Lateral habenula as a source of negative reward signals in
628 dopamine neurons. *Nature* **447**, 1111-1115, doi:10.1038/nature05860 (2007).

629 7 Grigsby, K. B., Kelty, T. J. & Booth, F. W. Medial habenula maturational deficits associate with
630 low motivation for voluntary physical activity. *Brain Res* **1698**, 187-194,
631 doi:10.1016/j.brainres.2018.08.016 (2018).

632 8 Hsu, Y. W. *et al.* Role of the dorsal medial habenula in the regulation of voluntary activity, motor
633 function, hedonic state, and primary reinforcement. *J Neurosci* **34**, 11366-11384,
634 doi:10.1523/JNEUROSCI.1861-14.2014 (2014).

635 9 Viswanath, H., Carter, A. Q., Baldwin, P. R., Molfese, D. L. & Salas, R. The medial habenula: still
636 neglected. *Front Hum Neurosci* **7**, 931, doi:10.3389/fnhum.2013.00931 (2013).

637 10 Cadd, G. & McKnight, G. S. Distinct patterns of cAMP-dependent protein kinase gene expression
638 in mouse brain. *Neuron* **3**, 71-79, doi:10.1016/0896-6273(89)90116-5 (1989).

639 11 London, E. *et al.* Differentially regulated protein kinase A (PKA) activity in adipose tissue and
640 liver is associated with resistance to diet-induced obesity and glucose intolerance in mice that
641 lack PKA regulatory subunit type IIalpha. *Endocrinology* **155**, 3397-3408, doi:10.1210/en.2014-
642 1122 (2014).

643 12 Lenard, N. R. & Berthoud, H. R. Central and peripheral regulation of food intake and physical
644 activity: pathways and genes. *Obesity (Silver Spring)* **16 Suppl 3**, S11-22,
645 doi:10.1038/oby.2008.511 (2008).

646 13 Boulos, L. J., Darcq, E. & Kieffer, B. L. Translating the Habenula-From Rodents to Humans. *Biol*
647 *Psychiatry* **81**, 296-305, doi:10.1016/j.biopsych.2016.06.003 (2017).

648 14 Volkow, N. D., Wang, G. J., Fowler, J. S., Tomasi, D. & Baler, R. Food and drug reward:
649 overlapping circuits in human obesity and addiction. *Curr Top Behav Neurosci* **11**, 1-24,
650 doi:10.1007/7854_2011_169 (2012).

651 15 Geisler, S. & Trimble, M. The lateral habenula: no longer neglected. *CNS Spectr* **13**, 484-489,
652 doi:10.1017/s1092852900016710 (2008).

653 16 Stamatakis, A. M. *et al.* Lateral Hypothalamic Area Glutamatergic Neurons and Their Projections
654 to the Lateral Habenula Regulate Feeding and Reward. *J Neurosci* **36**, 302-311,
655 doi:10.1523/JNEUROSCI.1202-15.2016 (2016).

656 17 Kim, U. & Chang, S. Y. Dendritic morphology, local circuitry, and intrinsic electrophysiology of
657 neurons in the rat medial and lateral habenular nuclei of the epithalamus. *J Comp Neurol* **483**,
658 236-250, doi:10.1002/cne.20410 (2005).

659 18 Hsu, Y. W. *et al.* Medial habenula output circuit mediated by alpha5 nicotinic receptor-
660 expressing GABAergic neurons in the interpeduncular nucleus. *J Neurosci* **33**, 18022-18035,
661 doi:10.1523/JNEUROSCI.2927-13.2013 (2013).

662 19 Quina, L. A., Wang, S., Ng, L. & Turner, E. E. Brn3a and Nurr1 mediate a gene regulatory pathway
663 for habenula development. *J Neurosci* **29**, 14309-14322, doi:10.1523/JNEUROSCI.2430-09.2009
664 (2009).

665 20 Contestabile, A. *et al.* Topography of cholinergic and substance P pathways in the habenulo-
666 interpeduncular system of the rat. An immunocytochemical and microchemical approach.
667 *Neuroscience* **21**, 253-270, doi:10.1016/0306-4522(87)90337-x (1987).

668 21 Lecourtier, L. & Kelly, P. H. A conductor hidden in the orchestra? Role of the habenular complex
669 in monoamine transmission and cognition. *Neurosci Biobehav Rev* **31**, 658-672,
670 doi:10.1016/j.neubiorev.2007.01.004 (2007).

671 22 Ren, J. *et al.* Habenula "cholinergic" neurons co-release glutamate and acetylcholine and
672 activate postsynaptic neurons via distinct transmission modes. *Neuron* **69**, 445-452,
673 doi:10.1016/j.neuron.2010.12.038 (2011).

674 23 Authement, M. E. *et al.* A role for corticotropin-releasing factor signaling in the lateral habenula
675 and its modulation by early-life stress. *Sci Signal* **11**, doi:10.1126/scisignal.aan6480 (2018).

676 24 Biran, J., Palevitch, O., Ben-Dor, S. & Levavi-Sivan, B. Neurokinin Bs and neurokinin B receptors
677 in zebrafish-potential role in controlling fish reproduction. *Proc Natl Acad Sci U S A* **109**, 10269-
678 10274, doi:10.1073/pnas.1119165109 (2012).

679 25 Hu, F., Ren, J., Zhang, J. E., Zhong, W. & Luo, M. Natriuretic peptides block synaptic transmission
680 by activating phosphodiesterase 2A and reducing presynaptic PKA activity. *Proc Natl Acad Sci U S*
681 *A* **109**, 17681-17686, doi:10.1073/pnas.1209185109 (2012).

682 26 Burton, K. A. *et al.* Type II regulatory subunits are not required for the anchoring-dependent
683 modulation of Ca²⁺ channel activity by cAMP-dependent protein kinase. *Proc Natl Acad Sci U S*
684 *A* **94**, 11067-11072, doi:10.1073/pnas.94.20.11067 (1997).

685 27 Geisler, S., Derst, C., Veh, R. W. & Zahm, D. S. Glutamatergic afferents of the ventral tegmental
686 area in the rat. *J Neurosci* **27**, 5730-5743, doi:10.1523/JNEUROSCI.0012-07.2007 (2007).

687 28 Aizawa, H., Kobayashi, M., Tanaka, S., Fukai, T. & Okamoto, H. Molecular characterization of the
688 subnuclei in rat habenula. *J Comp Neurol* **520**, 4051-4066, doi:10.1002/cne.23167 (2012).

689 29 Wallace, M. L. *et al.* Anatomical and single-cell transcriptional profiling of the murine habenular
690 complex. *Elife* **9**, doi:10.7554/eLife.51271 (2020).

691 30 Amieux, P. S. *et al.* Compensatory regulation of RIalpha protein levels in protein kinase A mutant
692 mice. *J Biol Chem* **272**, 3993-3998, doi:10.1074/jbc.272.7.3993 (1997).

693 31 Yang, L., Gilbert, M. L., Zheng, R. & McKnight, G. S. Selective expression of a dominant-negative
694 type Ialpha PKA regulatory subunit in striatal medium spiny neurons impairs gene expression
695 and leads to reduced feeding and locomotor activity. *J Neurosci* **34**, 4896-4904,
696 doi:10.1523/JNEUROSCI.3460-13.2014 (2014).

697 32 Sutherland, R. J. The dorsal diencephalic conduction system: a review of the anatomy and
698 functions of the habenular complex. *Neurosci Biobehav Rev* **6**, 1-13, doi:10.1016/0149-
699 7634(82)90003-3 (1982).

700 33 Hikosaka, O., Sesack, S. R., Lecourtier, L. & Shepard, P. D. Habenula: crossroad between the
701 basal ganglia and the limbic system. *J Neurosci* **28**, 11825-11829, doi:10.1523/JNEUROSCI.3463-
702 08.2008 (2008).

703 34 Bischoff, S. *et al.* Spatial distribution of GABA(B)R1 receptor mRNA and binding sites in the rat
704 brain. *J Comp Neurol* **412**, 1-16 (1999).

705 35 Charles, K. J. *et al.* Comparative immunohistochemical localisation of GABA(B1a), GABA(B1b)
706 and GABA(B2) subunits in rat brain, spinal cord and dorsal root ganglion. *Neuroscience* **106**, 447-
707 467, doi:10.1016/s0306-4522(01)00296-2 (2001).

708 36 Hudson, J. I., Hiripi, E., Pope, H. G., Jr. & Kessler, R. C. The prevalence and correlates of eating
709 disorders in the National Comorbidity Survey Replication. *Biol Psychiatry* **61**, 348-358,
710 doi:10.1016/j.biopsych.2006.03.040 (2007).

711 37 Klump, K. L., Racine, S., Hildebrandt, B. & Sisk, C. L. Sex differences in binge eating patterns in
712 male and female adult rats. *Int J Eat Disord* **46**, 729-736, doi:10.1002/eat.22139 (2013).

713 38 Wise, R. A., Spindler, J. & Legault, L. Major attenuation of food reward with performance-sparing
714 doses of pimozone in the rat. *Can J Psychol* **32**, 77-85, doi:10.1037/h0081678 (1978).

715 39 Wise, R. A. Dopamine, learning and motivation. *Nat Rev Neurosci* **5**, 483-494,
716 doi:10.1038/nrn1406 (2004).

717 40 Geiger, B. M. *et al.* Deficits of mesolimbic dopamine neurotransmission in rat dietary obesity.
718 *Neuroscience* **159**, 1193-1199, doi:10.1016/j.neuroscience.2009.02.007 (2009).

719 41 Sharma, S. & Fulton, S. Diet-induced obesity promotes depressive-like behaviour that is
720 associated with neural adaptations in brain reward circuitry. *Int J Obes (Lond)* **37**, 382-389,
721 doi:10.1038/ijo.2012.48 (2013).

722 42 Svenningsson, P. *et al.* DARPP-32: an integrator of neurotransmission. *Annu Rev Pharmacol*
723 *Toxicol* **44**, 269-296, doi:10.1146/annurev.pharmtox.44.101802.121415 (2004).

724 43 Teegarden, S. L., Nestler, E. J. & Bale, T. L. Delta FosB-mediated alterations in dopamine signaling
725 are normalized by a palatable high-fat diet. *Biol Psychiatry* **64**, 941-950,
726 doi:10.1016/j.biopsych.2008.06.007 (2008).

727 44 Rada, P., Bocarsly, M. E., Barson, J. R., Hoebel, B. G. & Leibowitz, S. F. Reduced accumbens
728 dopamine in Sprague-Dawley rats prone to overeating a fat-rich diet. *Physiol Behav* **101**, 394-
729 400, doi:10.1016/j.physbeh.2010.07.005 (2010).

730 45 Svenningsson, P. *et al.* Involvement of striatal and extrastriatal DARPP-32 in biochemical and
731 behavioral effects of fluoxetine (Prozac). *Proc Natl Acad Sci U S A* **99**, 3182-3187,
732 doi:10.1073/pnas.052712799 (2002).

733 46 Liu, M. Y. *et al.* Sucrose preference test for measurement of stress-induced anhedonia in mice.
734 *Nat Protoc* **13**, 1686-1698, doi:10.1038/s41596-018-0011-z (2018).

735 47 Nieh, E. H. *et al.* Decoding neural circuits that control compulsive sucrose seeking. *Cell* **160**, 528-
736 541, doi:10.1016/j.cell.2015.01.003 (2015).

737 48 Grant, J. Tachykinins stimulate a subset of mouse taste cells. *PLoS One* **7**, e31697,
738 doi:10.1371/journal.pone.0031697 (2012).

739 49 Yoo, J. H. *et al.* Ventral tegmental area glutamate neurons co-release GABA and promote
740 positive reinforcement. *Nat Commun* **7**, 13697, doi:10.1038/ncomms13697 (2016).

741 50 Paul, M. J., Indic, P. & Schwartz, W. J. A role for the habenula in the regulation of locomotor
742 activity cycles. *Eur J Neurosci* **34**, 478-488, doi:10.1111/j.1460-9568.2011.07762.x (2011).

743 51 Rhodes, J. S., Garland, T., Jr. & Gammie, S. C. Patterns of brain activity associated with variation
744 in voluntary wheel-running behavior. *Behav Neurosci* **117**, 1243-1256, doi:10.1037/0735-
745 7044.117.6.1243 (2003).

746 52 Febbraro, F., Svenningsen, K., Tran, T. P. & Wiborg, O. Neuronal substrates underlying stress
747 resilience and susceptibility in rats. *PLoS One* **12**, e0179434, doi:10.1371/journal.pone.0179434
748 (2017).

749 53 Cullinan, W. E., Herman, J. P., Battaglia, D. F., Akil, H. & Watson, S. J. Pattern and time course of
750 immediate early gene expression in rat brain following acute stress. *Neuroscience* **64**, 477-505,
751 doi:10.1016/0306-4522(94)00355-9 (1995).

752 54 Matsumoto, M. & Hikosaka, O. Representation of negative motivational value in the primate
753 lateral habenula. *Nat Neurosci* **12**, 77-84, doi:10.1038/nn.2233 (2009).

754 55 Szczypinski, J. J. & Gola, M. Dopamine dysregulation hypothesis: the common basis for
755 motivational anhedonia in major depressive disorder and schizophrenia? *Rev Neurosci* **29**, 727-
756 744, doi:10.1515/revneuro-2017-0091 (2018).

757 56 Sartorius, A. & Henn, F. A. Deep brain stimulation of the lateral habenula in treatment resistant
758 major depression. *Med Hypotheses* **69**, 1305-1308, doi:10.1016/j.mehy.2007.03.021 (2007).

759 57 Hankir, M. K. *et al.* Gastric Bypass Surgery Recruits a Gut PPAR-alpha-Striatal D1R Pathway to
760 Reduce Fat Appetite in Obese Rats. *Cell Metab* **25**, 335-344, doi:10.1016/j.cmet.2016.12.006
761 (2017).

762 58 London, E., Bloyd, M. & Stratakis, C. A. PKA functions in metabolism and resistance to obesity:
763 lessons from mouse and human studies. *J Endocrinol* **246**, R51-R64, doi:10.1530/JOE-20-0035
764 (2020).

765 59 Carrier, N. & Kabbaj, M. Sex differences in the antidepressant-like effects of ketamine.
766 *Neuropharmacology* **70**, 27-34, doi:10.1016/j.neuropharm.2012.12.009 (2013).

767 60 Kessler, R. C. Epidemiology of women and depression. *J Affect Disord* **74**, 5-13,
768 doi:10.1016/s0165-0327(02)00426-3 (2003).

769 61 Keers, R. & Aitchison, K. J. Gender differences in antidepressant drug response. *Int Rev*
770 *Psychiatry* **22**, 485-500, doi:10.3109/09540261.2010.496448 (2010).

771 62 Carmona, N. E. *et al.* Sex differences in the mediators of functional disability in Major Depressive
772 Disorder. *J Psychiatr Res* **96**, 108-114, doi:10.1016/j.jpsychires.2017.09.025 (2018).

773 63 Antolin-Fontes, B., Ables, J. L., Gorlich, A. & Ibanez-Tallon, I. The habenulo-interpeduncular
774 pathway in nicotine aversion and withdrawal. *Neuropharmacology* **96**, 213-222,
775 doi:10.1016/j.neuropharm.2014.11.019 (2015).

776 64 Han, S. *et al.* Down-regulation of cholinergic signaling in the habenula induces anhedonia-like
777 behavior. *Sci Rep* **7**, 900, doi:10.1038/s41598-017-01088-6 (2017).

778 65 Volkow, N. D., Koob, G. F. & McLellan, A. T. Neurobiologic Advances from the Brain Disease
779 Model of Addiction. *N Engl J Med* **374**, 363-371, doi:10.1056/NEJMr1511480 (2016).

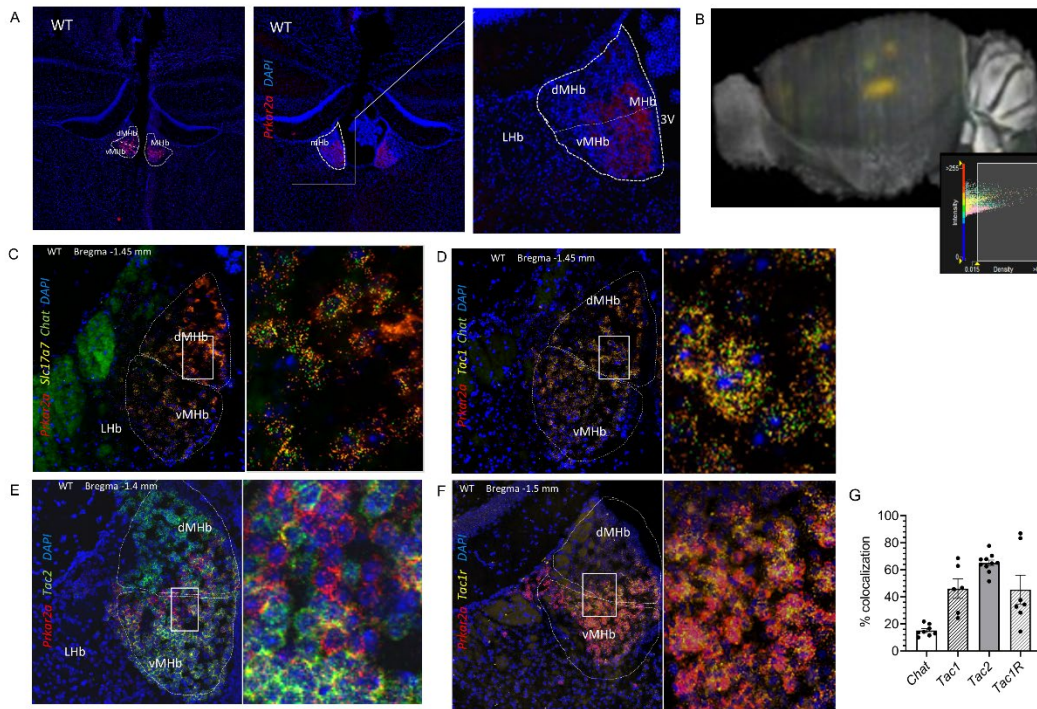
780 66 Robinson, T. E. & Berridge, K. C. The neural basis of drug craving: an incentive-sensitization
781 theory of addiction. *Brain Res Brain Res Rev* **18**, 247-291, doi:10.1016/0165-0173(93)90013-p
782 (1993).

783 67 Paxinos, G., Franklin, K. B. J. & Franklin, K. B. J. *The mouse brain in stereotaxic coordinates*. 2nd
784 edn, (Academic Press, 2001).

785 68 Nesterova, M., Yokozaki, H., McDuffie, E. & Cho-Chung, Y. S. Overexpression of RII beta
786 regulatory subunit of protein kinase A in human colon carcinoma cell induces growth arrest and
787 phenotypic changes that are abolished by site-directed mutation of RII beta. *Eur J Biochem* **235**,
788 486-494, doi:10.1111/j.1432-1033.1996.00486.x (1996).

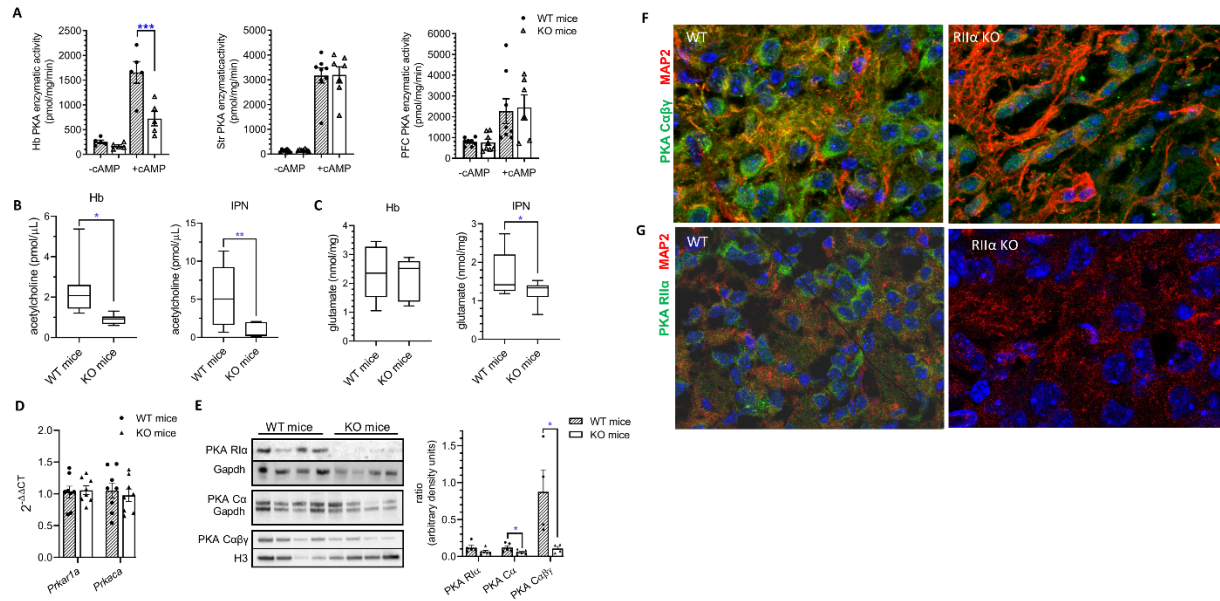
789 69 Livak, K. J. & Schmittgen, T. D. Analysis of relative gene expression data using real-time
790 quantitative PCR and the 2⁻(Delta Delta C(T)) Method. *Methods* **25**, 402-408,
791 doi:10.1006/meth.2001.1262 (2001).

792 70 Everett, M. Acquiring and Analyzing Data for Colocalization Experiments in AIM or ZEN Software.
793 (2011).



795

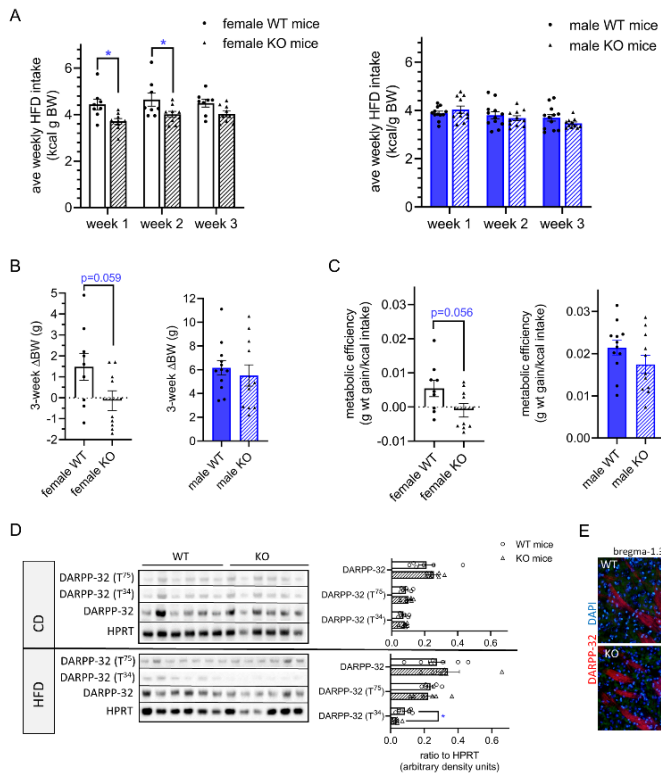
796 **Figure 1.** In brain, *Prkar2a* expression is nearly exclusive to habenula. A. *In situ* hybridization (ISH) for
 797 *Prkar2a* (left) and immunofluorescence (IF) for PKA RII α protein (right) with higher magnification detail
 798 show that expression in WT (C57/Bl6) mouse brain is primarily in the MHb, and B. 3-D ISH for *Prkar2a*
 799 shows robust and specific habenular localization of *Prkar2a* (3-D image: Allen Brain Institute).
 800 Representative ISH images (and higher magnification details) show colocalization of *Prkar2a* with C.
 801 *Slc17a7* and *Chat*, D. *Tac1* and *Chat*, E. *Tac2* and F. *Tac1R* in dMHb and VMHb. G. In MHb, *Chat*, *Tac1*,
 802 *Tac2* and *Tac1R* were expressed in approximately 15%, 46%, 65%, and 40% of *Prkar2a* expressing cells;
 803 n=6-11 sections from 3 different mice (1 male, 2 female) for each target; two-tailed unpaired t-tests; *,
 804 p< 0.05. All data represent the mean \pm sem.



805

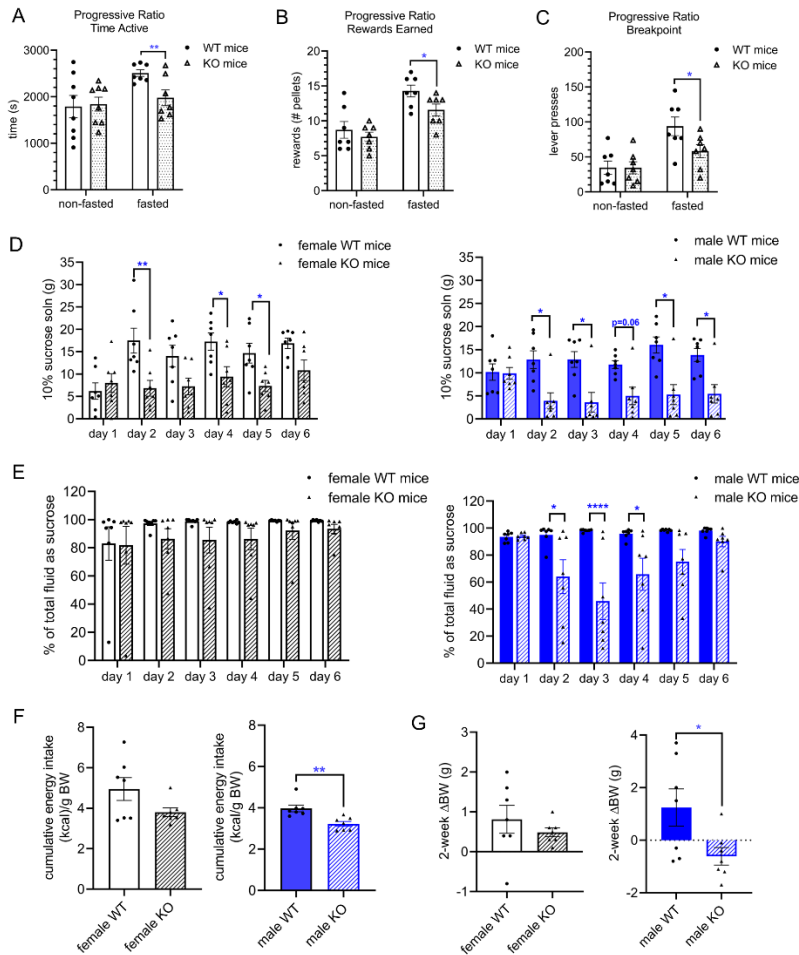
806 **Figure 2.** RIIαKO mice had reduced habenular PKA enzymatic activity, decreased interpeduncular
807 nucleus (IPN) acetylcholine and glutamate levels and altered localization of PKA catalytic subunit to
808 dendrites compared to WT mice. A. Basal and total (cAMP-stimulated) PKA enzymatic activities in Hb,
809 striatum (Str) and prefrontal cortex (PFC); n=5-8/group (female data shown); ***, $P < 0.0001$, unpaired
810 two-tailed t-tests, B. Acetylcholine concentrations in Hb and IPN were lower in RIIαKO mice compared to
811 WT littermates; n=6-7/sex/group (male data shown); **, $p < 0.01$, unpaired two-tailed t-test. C.
812 Glutamate concentrations did not differ in Hb but were lower in IPN of KO compared to WT mice; n=7-
813 9/group (female (Hb) and male data (IPN) shown), *, $p < 0.05$, unpaired two-tailed t-test, D. Habenular
814 *Prkar1a* and *Prkaca* mRNA levels did not differ between WT and RIIαKO mice; n=7/group (male data
815 shown), unpaired two-tailed t-tests, D. Representative western blots of Hb lysates for PKA subunits RIIα
816 and Cα (first membrane with Gapdh as housekeeper, females) and combined Cαβγ (second membrane
817 with Histone 3 as housekeeper, males); n=4/genotype; unpaired two-tailed t-tests, *, $p < 0.05$.
818 Representative immunofluorescent images of WT (left) and RIIαKO (right) brain sections (MHb) showed
819 differences in the subcellular localization of: E. PKA catalytic subunits (αβγ, green) in lower dMHb in WT,

820 and mutant mice that had impaired dendritic localization (shown by staining for MAP2, red), and F. PKA
821 RII α (green) that is localized both to the cell body and dendrites (MAP2, red) in WT mice (female data
822 shown). All data represent the mean \pm sem.



823

824 **Figure 3.** RII α KO mice had decreased HFD intake, sucrose solution intake and sucrose preference
 825 compared to WT mice and differences were influenced by sex. A. Average weekly intake of HFD during a
 826 3-week period of *ad libitum* access was adjusted for body weight; n= 8–12/sex/genotype; repeated
 827 measure two-way ANOVA with multiple comparisons (Bonferroni post hoc test). B. Difference in BW
 828 (Δ BW) from outset of HFD intake experiment until the end of wk3 (1 negative data point for MKO not
 829 shown on graph); n= 8–12/sex/genotype; two-way unpaired t-test; n= 8–12/sex/genotype, and C.
 830 metabolic efficiency (kcal intake/wt gain) for female and male RII α KO and WT mice during 3wk HFD-
 831 feeding period (1 negative data point for FKO not shown on graph); n=9-12/sex/group, two-way
 832 unpaired t-test. D. Representative western blot of striatal lysates from mice fed CD (top) or HFD (3wk)
 833 (bottom) for DARPP-32 and DARPP-32 (T³⁴) with HPRT as the loading control and densitometry analysis;
 834 two-way unpaired t-test, female data shown; E. Representative IF image of post-HFD (3wk) striatum
 835 probed for DARPP-32 and counterstained with DAPI (n=3 mice/genotype, females).

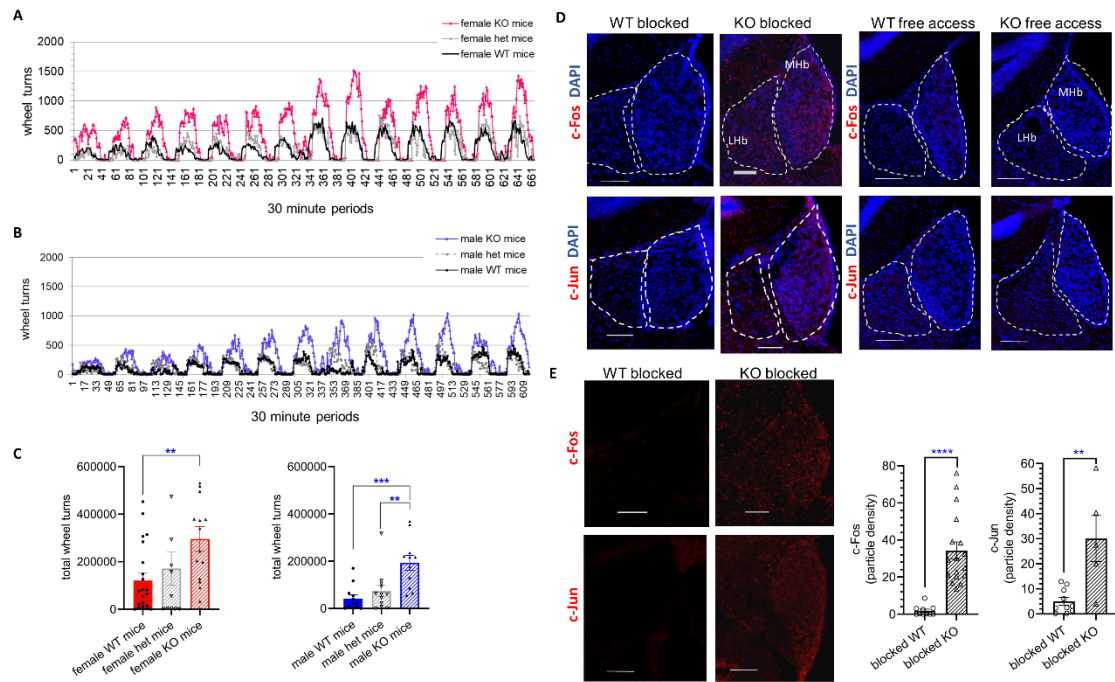


836

837 Figure 4. RII α KO mice had decreased motivation for food rewards, decreased sucrose solution intake
 838 and sucrose preference compared to WT mice; differences were influenced by sex. A. Amount of time
 839 spent engaged in a progressive ratio operant task, B. breakpoint, and C. number of food pellets earned
 840 by WT and RII α KO littermates during progressive ratio operant task in fed and fasted states, n= 7-
 841 8/group, (female mice), analyzed by unpaired two-way t-tests. D. Average daily intake of 10% sucrose
 842 solution of female and male RII α KO and WT mice; repeated measure two-way ANOVA with multiple
 843 comparisons (Bonferroni post hoc test); and E. sucrose preference ((daily sucrose solution intake
 844 (g)/total fluid intake (g)) X 100); sucrose intake and preference analyzed by repeated measure two-way
 845 ANOVA with multiple comparisons (Bonferroni post hoc test). F. Cumulative total energy intake adjusted
 846 for body weight for female and male mice during 2wk experiment, ((sucrose kcal + chow kcal)/ g BW),

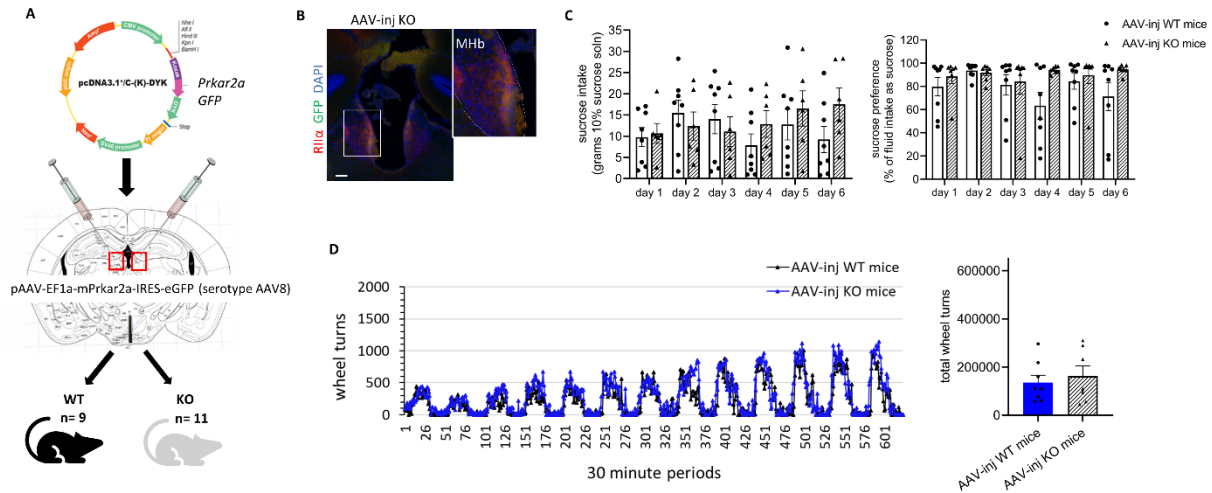
847 analyzed by two-way unpaired t-test (male) and Mann Whitney non-parametric rank test (female), and
848 G. Change in body weight during the 2wk sucrose intake experiment, analyzed by two-way unpaired t-
849 test (male) and Mann Whitney (female). For sucrose studies, n=9-12/sex/group. All data are mean \pm
850 sem; *, $P < 0.05$; **, $P < 0.01$, ****, $P < 0.0001$.

851



852

853 **Figure 5.** RII α KO mice run more than twice the distance as their WT littermates during home cage
854 running wheel access. Heterozygosity for *Prkar2a* rescued the running phenotype. Voluntary running
855 activity was graphed in bins of 30 minutes over a two-week period for A. female (n=11-24/genotype),
856 and B. male (n=8-12/genotype) RII α KO, RII α +/- and WT mice, and C. the total number of wheel turns
857 during the 2wk period, analyzed by one-way ANOVA with multiple comparisons (Bonferroni's post hoc
858 test). D. Representative staining for c-Fos or c-Jun (red) (merged with DAPI) in WT and RII α KO mice
859 either permitted to run as already acclimated for 2wk prior or blocked from running at the outset of the
860 dark cycle (1800h). E. The same images (4D) are shown with only c-Fos or c-Jun (red) and particle density
861 of c-Fos and c-Jun was analyzed with ImageJ software; unpaired two-way t-tests, n=5-17 sections from a
862 total 3-5 mice per IEG/genotype (3 males, 7 females). Particle density is defined as the number of
863 counted particles divided by the area ratio of the MHb, with the latter being the area of the MHb over
864 the total image area. All data represent mean \pm sem; scale bars represent 100 μ M; *, $P < 0.05$; **, $P <$
865 0.01, ***, $P < 0.001$, ****, $P < 0.0001$.



866

867 **Figure 6.** Stereotaxic rAAV-mediated re-expression of *Prkar2a* rescued the sucrose and running
 868 phenotypes of RII α KO mice. A. Map of *Prkar2a* expression vector used to generate injectable rAAV and
 869 diagram of the injection strategy, B. Representative image of coronal section from injected RII α KO
 870 mouse of a successful rAAV-injection with expression of RII α and GFP in MHB with magnified portion on
 871 right; scale bar represents 100 μ M, C. Sucrose intake and sucrose preference tests for rAAV-injected WT
 872 and KO mice revealed no differences between genotypes (n=6-8/group; 7 males, 7 females), and D. 2wk
 873 running wheel activity of rAAV-injected WT and KO mice did not differ between genotypes; (n=7-
 874 8/group; 6 males, 9 females), repeated measure two-way ANOVA with multiple comparisons
 875 (Bonferroni's post hoc test) and a two-tailed t-test were used for sucrose and running analyses,
 876 respectively; all data represent the mean \pm sem.